Available online at www.sciencedirect.com
ScienceDirect
Journal of Sound and Vibration 300 (2007) 25–42
JOURNAL OF SOUND AND VIBRATION
www.elsevier.com/locate/jsvi

Array technology for bending wave field analysis in constructions

A.J. Berkhout, Diemer de Vries*, Maarten C. Brink

Laboratory of Acoustical Imaging and Sound Control, Department of Imaging Science and Technology, Faculty of Applied Sciences, Delft University of Technology, P.O.B. 5046, 2600 GA Delft, The Netherlands

Received 18 February 2004; received in revised form 19 April 2006; accepted 29 June 2006
Available online 10 October 2006

Abstract

In this paper it is shown that array technology is an essential tool for the quantitative analysis of bending wave fields in elastic, solid constructions. The advantages can be compared with those of array-based acoustic wave field analysis in free air as well as in enclosed spaces. In contrast to acoustic waves, bending waves are highly dispersive, i.e., their propagation velocity depends strongly on frequency. A convolution operation is introduced as a preprocessing step, removing the dispersion from the bending waves, such that their propagation properties become highly similar to that of acoustic waves. After this transformation, multidimensional acoustic wave field analysis methods can be successfully applied to bending wave fields, using the large technology portfolio in acoustic imaging. The new analysis method is applied to simulated bending wave fields and to real measurements on a rectangular steel plate. The proposed method is demonstrated on bending wave fields, but it can be applied to any type of dispersive wave phenomenon.

1. Introduction

In the context of sound radiation by vibrating structures and sound transmission through partition walls, bending waves play a dominant role since their displacements are perpendicular to the construction such that they most efficiently couple to the acoustic field in the surrounding air. A widely used concept to describe, in more complex configurations as ships or buildings, the energy exchange between vibrating elements and air and the conversion between different wave types is the statistical energy analysis (SEA) model [1]. The model assumes that all relevant wave fields have a diffuse character, which is often doubtful in practice. And even if this assumption holds, the model describes the phenomena only in a statistical sense being unable to take the influence of local inhomogeneities into account. Therefore, it is desired to have, in addition to SEA-based information, more local information on the behavior of bending waves. A direct way to obtain more physical insight in the matter is to perform and analyze suitable measurements on representative structures. Time domain measurements on bars where the dispersive character of bending waves becomes evident have been reported already in the 1970s by Holmes [2]. Since then, many measurements on structures have been done

*Corresponding author. Fax: +31 15 2625403.
E-mail address: d.devries@tudelft.nl (D. de Vries).

0022-460X/$ - see front matter
doi:10.1016/j.jsv.2006.06.070

using impulsive impact source signals, in order to determine material properties such as damping (e.g. Ref. [3]) or to investigate the relation between vibration and sound radiation (e.g. Ref. [4]). In most applications, measurements were done on a few 'representative' positions. This way, distributed local information is obtained which can be processed in a statistical manner. This means that a deterministic approach is lacking until today.

In earlier papers it has been shown that application of array technology is a powerful tool for deterministic analysis of sound fields in enclosed spaces [5] and in outdoor situations [6]. Fig. 1 shows the multi-channel impulse response of a rectangular lecture room, measured every 5 cm along a linear array of microphone positions, half-way the hall over its full-width with the source front center. The results are displayed as a visual entity in the offset-traveltime domain: the abscissa shows the lateral microphone coordinate *re* the array center (the 'offset'), the ordinate the traveltime *re* the moment of pulse generation. The picture clearly reveals the direct and reflected wave fronts. Note that, in order to get a picture with highest temporal resolution, the shortest wavelet for the given amplitude spectrum is applied, i.e., the symmetric zero-phase wavelet that is obtained by deconvolution of the recorded data with the source signal [7].

A logical follow-up of the successful application of array technology to acoustic wave fields is its application to bending wave fields in elastic, solid structures in order to reveal their temporal and spatial properties in a deterministic way. However, a fundamental difference between bending and acoustic waves is that bending waves are highly dispersive and acoustic waves are largely non-dispersive. Due to the fact that the propagation velocity of bending waves increases with frequency, an impulsive excitation signal broadens when propagating. This means that the temporal resolution of the registration of a bending wave field strongly deteriorates with traveltime. We propose a wave theory-based preprocessing step which removes dispersion from bending waves, resulting in a representation highly similar to 2D acoustic waves. Next, the same analysis methods as earlier derived for acoustic waves [5,6] can be applied.

Recently, a research project funded by the Dutch technology foundation STW has been started where the proposed bending wave field analysis method will be used in several applications. At present, the bending wave propagation in multi-actuator flat panel loudspeaker arrays for wave field synthesis is investigated; the proposed dispersion removal operation is a useful tool in this context. Further applications are foreseen in the analysis of vibrations in building constructions, machines, musical instruments and the shallow earth subsurface.

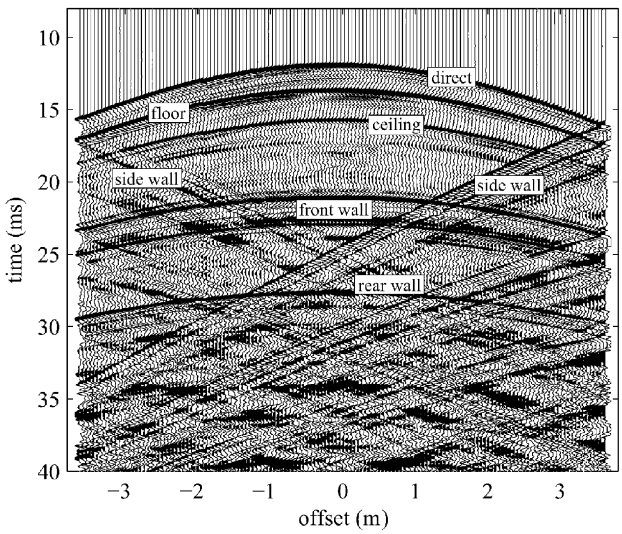

Fig. 1. Multi-channel impulse response measured in a lecture room along a linear detector array. The direct sound wave and the first-order reflections can easily be identified.

2. Bending waves in an infinite plate

A point force acting on a homogeneous elastic plate generates a 2D bending wave field, as illustrated in Fig. 2. The exact wave equation for the transversal displacement q of such a field cannot be given in closed form. When the thickness h of the plate is assumed to be small in comparison with the bending wavelength, shear displacements caused by shear forces may be neglected, which means that bending is described by pure rotation. If the rotation angles φ of vertical cross sections are sufficiently small such that $\tan(\varphi) \approx \varphi$, then the following approximate wave equation for the displacement q in the space–time domain due to a point force $\psi(t)$ positioned at (x_s, y_s) can be derived [8, Chapter 3]:

$$\nabla^4 q(x,y,t) + \frac{m''}{B'}\frac{\partial^2}{\partial t^2} q(x,y,t) = \frac{1}{B'}\psi(t)\delta(x-x_s)\delta(y-y_s) = -s_0(t)\delta(x-x_s)\delta(y-y_s), \tag{1a}$$

where m'' is the mass per unit area of the plate, given by $\rho_p h$ with ρ_p the density of the plate material, B' its bending stiffness per unit length, given by

$$B' = \frac{Eh^3}{12(1-\mu^2)}, \tag{1b}$$

E its Young modulus, μ its Poisson constant and

$$\nabla^4 = \left(\frac{\partial^2}{\partial x^2} + \frac{\partial^2}{\partial y^2}\right)^2. \tag{1c}$$

In the space–frequency domain the bending wave equation reads

$$\left(\nabla^4 - k_b^4\right) Q(x,y,\omega) = -S_0(\omega)\delta(x-x_s)\delta(y-y_s) \tag{2a}$$

or

$$\left(\nabla^2 - k_b^2\right)\left(\nabla^2 + k_b^2\right) Q(x,y,\omega) = -S_0(\omega)\delta(x-x_s)\delta(y-y_s), \tag{2b}$$

where $S_0(\omega)$ is the Fourier transform of $s_0(t)$.

The bending wavenumber is defined as

$$k_b = \frac{\omega}{c_b} \tag{2c}$$

with c_b being the propagation velocity for bending waves given by

$$c_b = c_b(\omega) = \sqrt{\omega}\sqrt[4]{\frac{Eh^2}{12\rho_p(1-\mu^2)}} = A\sqrt{\omega}. \tag{2d}$$

Eq. (2d) shows that the bending wave propagation velocity c_b increases with the square root of frequency, indicating that a bending wave field is dispersive. A is called the dispersion constant. Fig. 3 shows a graph of c_b as a function of frequency for a 30 mm steel plate.

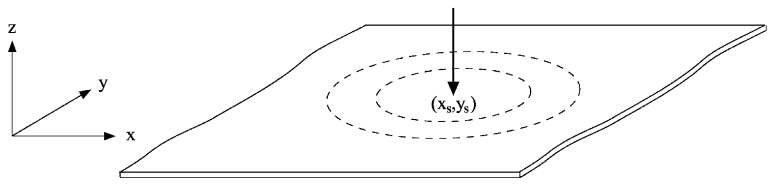

Fig. 2. Circular bending wave generated by a point force at (x_s, y_s) in an infinite plate.

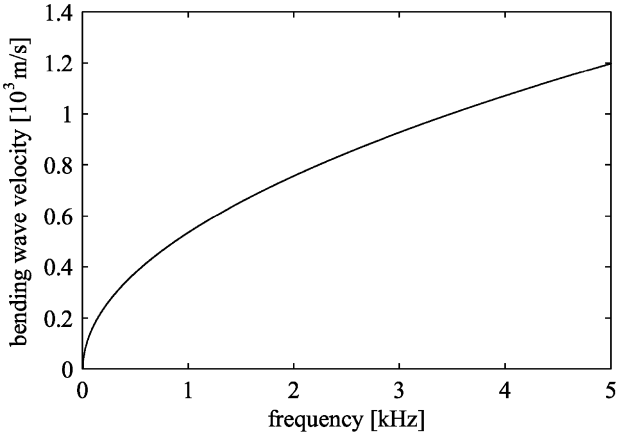

Fig. 3. Propagation velocity of bending waves as a function of frequency for a 30 mm thick steel plate.

Since the system is considered to be linear, Eq. (2b) can be decomposed into two sub-equations each having its specific source term:

$$\left(\nabla^2 - k_b^2\right) Q_1(x, y, \omega) = -S_1(\omega)\delta(x - x_s)\delta(y - y_s), \tag{3a}$$

$$\left(\nabla^2 + k_b^2\right) Q_2(x, y, \omega) = -S_2(\omega)\delta(x - x_s)\delta(y - y_s), \tag{3b}$$

such that its solution can be written as

$$Q(x, y, \omega) = Q_1(x, y, \omega) + Q_2(x, y, \omega), \tag{4a}$$

where $Q_1(x, y, \omega)$ represents an evanescent wave which can be neglected for $k_b r \gg 1$ and

$$Q_2(x, y, \omega) = \sqrt{\frac{2\mathrm{j}}{\pi k_b}}\left[S_1(\omega)\frac{\mathrm{e}^{-\mathrm{j}k_b r}}{\sqrt{r}}\right] \quad \text{for } k_b r \gg 1 \tag{4b}$$

with

$$r = \sqrt{(x - x_s)^2 + \left(y - y_s\right)^2}. \tag{4c}$$

Furthermore, it can be shown that with the substitution

$$S_b(\omega) = S_1(\omega)\sqrt{\frac{2\mathrm{j}}{\pi k_b}} = S_0(\omega)\sqrt{\frac{1}{32\mathrm{j}\pi k_b^5}} \tag{4d}$$

we can write

$$Q(x, y, \omega) = S_b(\omega)\frac{\mathrm{e}^{-\mathrm{j}(\omega/c_b(\omega))r}}{\sqrt{r}}, \tag{4e}$$

$c_b(\omega)$ being given by Eq. (2d).

Throughout this paper, simulations and measurements at an array of detector positions will be considered, positioned along the x-axis. Hence, the response at the nth detector in $(x_n, 0)$ can be written as

$$Q(x_n, 0, \omega) = Q(x_n, \omega) = S_b(\omega)\frac{\mathrm{e}^{-\mathrm{j}(\omega/c_b(\omega))r_n}}{\sqrt{r_n}} \tag{4f}$$

with

$$r_n = \sqrt{(x_n - x_s)^2 + y_s^2}. \tag{4g}$$

Note that, due to the dispersive character of the bending wave field, the inverse Fourier transform $q(x_n, t)$ of Eq. (4f) cannot be simply expressed in closed form.

The bending wave response of a bounded elastic plate due to a pulse emitted by a point force can be interpreted as the superposition of the signals of an infinite series of image sources, obtained by mirroring the primary source and its images in the boundaries. In the mirror image source space, source i at (x_i, y_i) has a distance r_{ni} to the nth detector of the array positioned at $(x_n, 0)$ given by

$$r_{ni} = \sqrt{(x_n - x_i)^2 + y_i^2}. \tag{5a}$$

Since the propagation velocity of bending waves c_b is dependent on frequency according to Eq. (2d), the signal of each source cannot be related to a distinct traveltime.

In the space–time domain, the bending wave response at the nth detector can be written as a summation of the contributions of the image sources, each 'labeled' by the distance r_{ni}:

$$q(x_n, t) = \sum_i q(r_{ni}; t). \tag{5b}$$

Due to the frequency-dependent propagation velocity, however, the mirror image source signals vary in a complex way and an analytic specification cannot simply be given. Therefore it is more relevant to write, in the space–frequency domain

$$Q(x_n, \omega) = \sum_i Q(r_{ni}; \omega), \tag{5c}$$

with, according to Eq. (4e),[1]

$$Q(r_{ni}; \omega) = \frac{S_b(\omega)\mathrm{e}^{-\mathrm{j}k_b r_{ni}}}{\sqrt{r_{ni}}} = \frac{S_b(\omega)\mathrm{e}^{-\mathrm{j}(\omega/c_b(\omega))r_{ni}}}{\sqrt{r_{ni}}}. \tag{5d}$$

In Section 4 a method is proposed to eliminate the dispersion from bending wave field data as described by Eq. (5d). The resulting data then have the form

$$\hat{Q}(r_{ni}; \omega) = \hat{S}(\omega)\frac{\mathrm{e}^{-\mathrm{j}(\omega/\hat{c})r_{ni}}}{\sqrt{r_{ni}}}. \tag{6a}$$

The notation $\hat{c}$ will be used throughout this paper to indicate dispersion-free versions of variables. The 'substitute' propagation velocity $\hat{c}$ is independent of frequency. The inverse Fourier transform of Eq. (6a) reads

$$\hat{q}(r_{ni}; t) = \frac{\hat{s}\left(t - r/\hat{c}\right)}{\sqrt{r_{ni}}}. \tag{6b}$$

It represents a transversal wave that preserves its original time domain signature when propagating, contrarily to the original bending wave.

3. Simulated array recordings

In this section, numerically *simulated* array recordings of bending wave responses in a 30 mm thick steel plate will be presented. Its bending wave propagation velocity c_b is displayed as a function of frequency in Fig. 3. The corresponding dispersion constant defined in Eq. (2d) is $6.76\,\mathrm{ms}^{-0.5}$. The source emits a zero-phase[2] signal with bandwidth 20–5 kHz.

[1] In principle, each mirror image source has a different source spectrum depending on the absorption coefficients of the boundaries in which the source has been mirrored. The source spectrum $S_b(r_{ni}; \omega)$ of image source i is related to the primary source spectrum $S_b(\omega)$ by multiplication with a reflectivity spectrum $R^b_{ni}(\omega)$: $S_b(r_{ni}; \omega) = R^b_{ni}(\omega)S_b(\omega)$, such that with Eq. (5d) $Q(r_{ni}; \omega) = \frac{R^b_{ni}(\omega)S_b(\omega)\mathrm{e}^{-\mathrm{j}(\omega/c_b(\omega))r_{ni}}}{\sqrt{r_{ni}}}$. However, for simplicity $R^b_{ni}(\omega)$ has been chosen 1 for all simulations in this paper.

[2] A zero-phase pulse is a symmetric signal, the phase spectrum of which is zero for all frequency components. For a given amplitude spectrum it has minimum length, and hence maximum resolution, in the time domain [7].

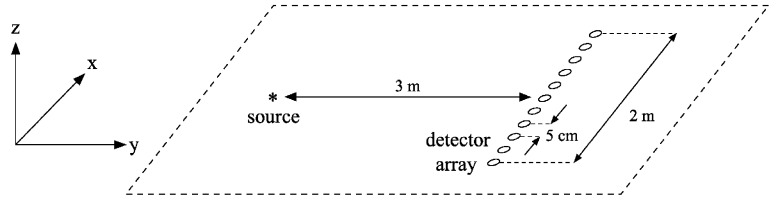

Fig. 4. Configuration of source and detector array as used in the simulation of Fig. 5 (not to scale).

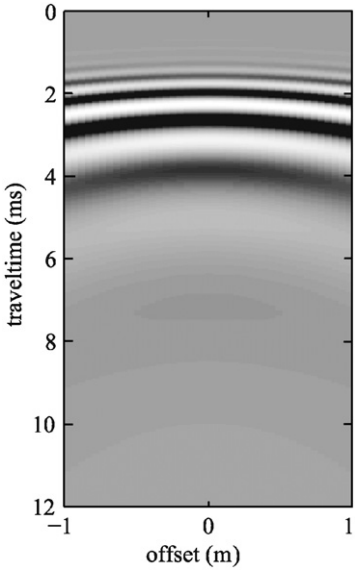

Fig. 5. Simulation of the bending wave response along a linear array on an unbounded steel plate (dispersion constant $A = 6.76\,\mathrm{ms}^{-0.5}$).

3.1. Free field array recording

For the simulation of a bending wave in an infinite plate, using Eq. (4f), the source is positioned in front of the center of a 2 m long detector array at a distance of 3 m (see Fig. 4).

In Fig. 5 the response is simulated at the detector array in the offset-traveltime domain. For each frequency component of the source signal the arrival times are defined by a hyperbola, the curvature of which is determined by the source-to-array distance and the propagation velocity. The propagation velocity is different for each frequency according to Eq. (2d), causing dispersion such that the time resolution of the data is increasingly worse for increasing source-to-array distance.

3.2. Bounded plate array recording

In Fig. 6, the responses along an array of detector positions are numerically simulated for a finite, rectangular steel plate with length 2.5 m and width 1.8 m. The source is positioned in the center of the plate, 0.75 m in front of a detector array covering the full plate width. The edges are taken free floating and fully reflective. The configuration closely resembles that of the configuration used for the measurements discussed in Section 5, shown in Fig. 12; the source was positioned at position s_4 in that figure.[3]

It is seen that, as expected, a very poor time resolution is obtained, such that the different wave fronts cannot be distinguished; effective wave field analysis is not possible in this situation. Our solution to this

[3]The configuration has been chosen such that the assumption that evanescent waves can be neglected—see Eq. (4b)—is satisfactorily fulfilled.

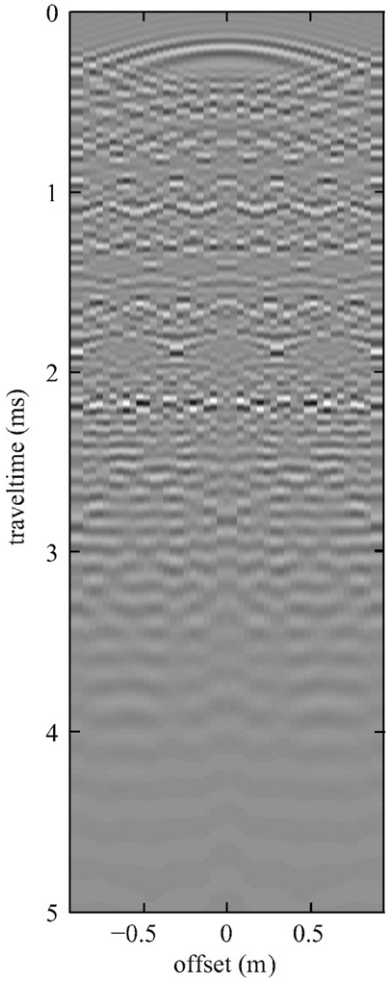

Fig. 6. Numerically simulated bending wave response for steel. Note the complex interference patterns due to boundary reflections.

problem is to apply, before analysis, a convolution operator that transforms the bending waves into dispersion-free waves. This operator is derived in the next section.

4. Dispersion removal from bending waves

4.1. Time-invariant convolution

We presume that we *know* the propagation velocity $c_b(\omega)$ of the medium as a function of frequency ('the model'). For the bending waves considered here the model is given by Eq. (2d).

In order to transfer the bending wave contribution $Q(r_{ni}; \omega)$ of (image) source i to array detector n into a dispersion-free wave $\hat{Q}(r_{ni}; \omega)$ we have to multiply it with a filter $F(r_{ni}; \omega)$ such that

$$\hat{Q}(r_{ni}; \omega) = F(r_{ni}; \omega) Q(r_{ni}; \omega). \tag{7a}$$

Using Eqs. (5d), (6a) we write

$$F(r_{ni}; \omega) = \frac{\hat{Q}(r_{ni}; \omega)}{Q(r_{ni}; \omega)} = \frac{\hat{S}(r_{ni}; \omega)}{S_b(r_{ni}; \omega)} e^{j\left((\omega/c_b)-(\omega/\hat{c})\right) r_{ni}}. \tag{7b}$$

We do not want to modify the amplitude spectrum of the bending waves when removing the dispersion, meaning that for each frequency component within the source signal bandwidth we choose $\hat{S}(r_{ni};\omega) = S_b(r_{ni};\omega)$.

$$F(r_{ni};\omega) = e^{j(\omega/c_b - \omega/\hat{c})r_{ni}}. \tag{7c}$$

Instead of r_{ni}, we can use any parameter that is unambiguously related to the source-to-detector distance as a 'label' for F, Q and $\hat{Q}$. Since the filtered result is a dispersion-free wave traveling between source and detector with frequency-independent 'substitute' propagation velocity $\hat{c}$ we can write

$$r_{ni} = \hat{c}t_{ni}, \tag{7d}$$

and rewrite Eq. (7b) as

$$F(t_{ni};\omega) = e^{j\omega((\hat{c}/c_b)-1)t_{ni}} = e^{j\omega((\hat{c}/c_b))t_{ni}} e^{-j\omega t_{ni}} = G(t_{ni};\omega)e^{-j\omega t_{ni}}, \tag{7e}$$

now using traveltime t_{ni} as a label. It should be realized that, by introducing $\hat{c}$ and Eq. (7d), we rescale the 'real' time domain t to a 'substitute' time domain $\hat{t}$ where dispersion-free versions of bending waves propagate. In this domain, t_{ni} is the traveltime between source i and receiver n.

The performance of filter $F(t_{ni};\omega)$ when applied to a bending wave according to Eq. (7a) is illustrated in Fig. 7. For the numerical parameter values, the following rather arbitrary choice has been made: source-to-receiver distance $r_{ni} = 5\,\mathrm{m}$, central source spectrum frequency $f_c = 2.5\,\mathrm{kHz}$, dispersion constant $A = 6.76\,\mathrm{ms}^{-0.5}$ and substitute velocity $\hat{c} = 1300\,\mathrm{m/s}$. Fig. 7(a) shows the amplitude spectrum and phase spectrum of bending wave $Q(t_{ni};\omega)$ which represents the input data. Due to the dispersive character, the phase spectrum of the input data is nonlinear. Fig. 7(b) shows the amplitude and phase spectra of the filter $G(t_{ni};\omega)$. It is seen that the amplitude spectrum of $G(t_{ni};\omega)$ is flat within the bandwidth of the input data, leaving the amplitude information of the input data unaffected. Its phase spectrum is the inverse of that of $Q(t_{ni};\omega)$. Therefore, $G(t_{ni};\omega)$ is the complex conjugate of a 'whitened' version of the input data, denoted as $Q_w(t_{ni};\omega)$. Multiplication of $Q(t_{ni};\omega)$ with $G(t_{ni};\omega)$ leaves the amplitude spectrum of the input data unchanged and yields a zero-phase spectrum. The result is a dispersion-free signal; see Fig. 7(c). Finally, by multiplication with the phase factor $e^{-j\omega t_{ni}}$, a linear phase spectrum is assigned to the zero-phase signal corresponding with a time shift from zero to the acoustic traveltime t_{ni} being 3.85 ms in this example. Fig. 7(d) shows the amplitude and phase spectra of the resulting dispersion-free version $\hat{Q}(t_{ni};\omega)$ of the input data.

Note that, after substitution of $r_{ni} = \hat{c}t_{ni}$, we can write Eq. (7a) in the time domain as a convolution:

$$\hat{q}(t_{ni};t) = f(t_{ni};t) * q(t_{ni};t) = g(t_{ni};t - t_{ni}) * q(t_{ni};t), \tag{7f}$$

or, in full notation:

$$\begin{aligned}\hat{q}(t_{ni};\hat{t}) &= \int_{-\infty}^{+\infty} f(t_{ni};\hat{t}-t)q(t_{ni};t)\,dt \\ &= \int_{-\infty}^{+\infty} g(t_{ni};\hat{t}-t-t_{ni})q(t_{ni};t)\,dt \\ &= \int_{-\infty}^{+\infty} q_w(t_{ni};t-\hat{t}+t_{ni})q(t_{ni};t)\,dt.\end{aligned} \tag{7g}$$

Note that $\hat{q}(t_{ni};\hat{t})$, $f(t_{ni};t)$, $g(t_{ni};t)$ and $q(t_{ni};t)$ are the inverse Fourier transforms of $\hat{Q}(t_{ni};\omega)$, $F(t_{ni};\omega)$, $G(t_{ni};\omega)$ and $Q(t_{ni};\omega)$, respectively. Note that the dispersion-free wavelet $\hat{q}$ is now written in the substitute time domain. In addition to the frequency domain description in Fig. 7, the dispersion removal procedure in the time domain is illustrated in Fig. 8, for the same numerical values.

Fig. 8(a) shows the dispersive bending wavelet in the time domain $q(t_{ni};t)$ representing the input data. Since, as was seen in Figs. 7(a) and (b), the zero-phasing operator $g(t_{ni};t)$ has about the same bandwidth and an inverse phase spectrum as compared to the input data, it is expected that it resembles a time-reversed version of $q(t_{ni};t)$ and, hence, that the time-reversed version $g(t_{ni};-t)$ of the zero-phasing operator resembles the input data $q(t_{ni};t)$ itself. This is confirmed by Fig. 8(b). We write

$$g(t_{ni};-t) = q_w(t_{ni};t), \tag{7h}$$

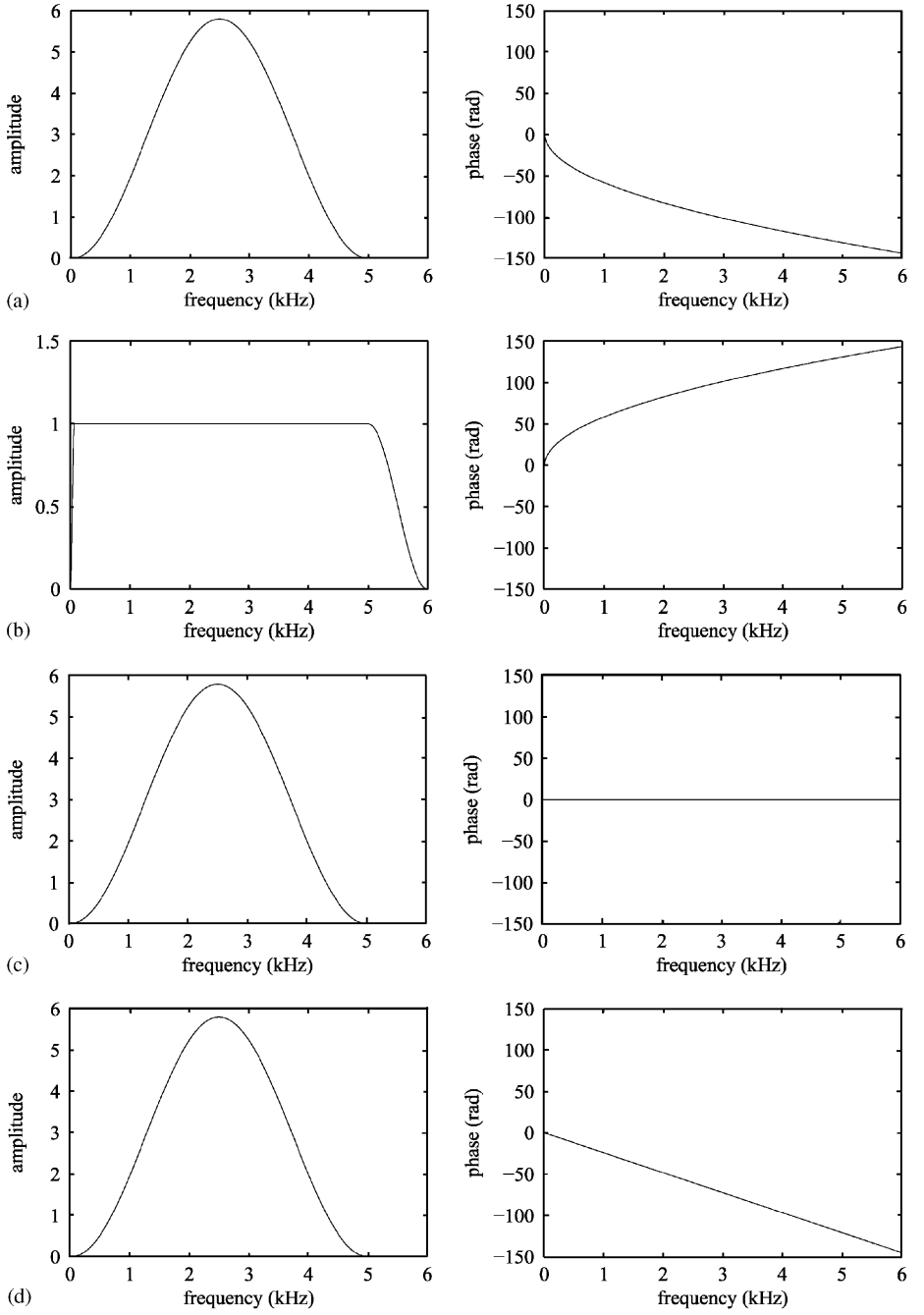

Fig. 7. Illustration of the performance of the dispersion removal filter $F(t_{ni}; w) = G(t_{ni}; w)e^{-j\omega t_{ni}}$ as specified in Eq. (7e). (a) Amplitude spectrum (left) and phase spectrum (right) of bending wave $Q(t_{ni}; \omega)$, (b) amplitude spectrum (left) and phase spectrum (right) of zero-phasing filter $G(t_{ni}; \omega) = Q_w^*(t_{ni}; \omega)$, (c) amplitude spectrum (left) and phase spectrum (right) of zero-phase result $G(t_{ni}; \omega)Q(t_{ni}; \omega)$ and (d) amplitude spectrum (left) and phase spectrum (right) of the resulting substitute wave component $P(t_{ni}; \omega) = F(t_{ni}; \omega)Q(t_{ni}; \omega)$.

where $q_w(t_{ni}; t)$ is a 'whitened' version of $q(t_{ni}; t)$. Fig. 8(c) shows the result of convolving input data $q(t_{ni}; t)$ with zero-phasing operator $g(t_{ni}; t)$, which can also be interpreted as taking the inner product of the input wavelet with a whitened version of itself. As expected, the result is a zero-phase pulse at substitute traveltime $\hat{t} = 0$. Fig. 8(d) shows the dispersion-free wavelet $\hat{q}(t_{ni}; \hat{t})$ that results when the full convolution of Eq. (7g),

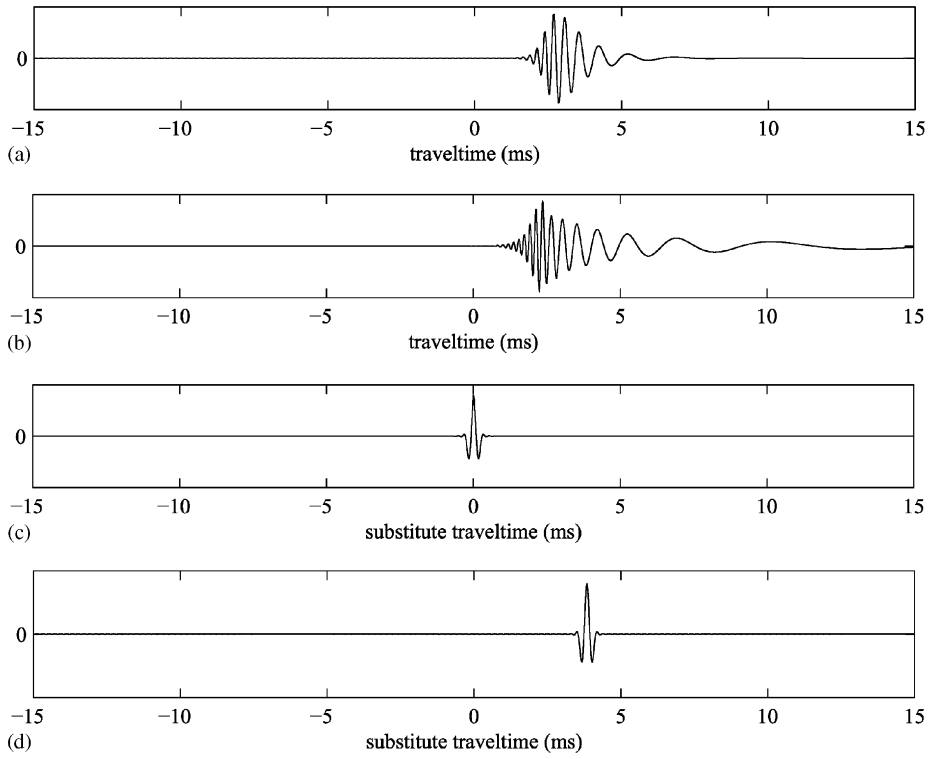

Fig. 8. Illustration of the performance of the dispersion removal convolution as specified in Eq. (7g). (a) Bending wavelet $q(t_{ni};\ t)$, (b) time-reversed zero-phasing operator $g(t_{ni};\ -t) = q_w(t_{ni};\ t)$, (c) zero-phase result $g(t_{ni};\ t) * q(t_{ni};\ t)$; * denotes convolution and (d) dispersion-free wavelet.

including the time shift corresponding with the source-to-receiver distance, is applied. As expected, it is a zero-phase wavelet positioned on its correct substitute traveltime position $\hat{t} = t_{ni} = 3.85\,\text{ms}$.

Since in processing practice always discrete values of t and $\hat{t}$ are used, Eq. (7f) can also be written in vector–matrix notation, for each detector array element n:

$$\hat{\mathbf{Q}}_n = \mathbf{F}\mathbf{Q}_n, \tag{7i}$$

where column vector $\mathbf{Q}_n$ contains the data points of input wavelet $q(t_{ni};\ t)$, the rows of matrix $\mathbf{F}$ contain, for subsequent values of $\hat{t}$, the shifted wavelets $q_w\left(t_{ni};\ t - \hat{t} + t_{ni}\right)$ and column vector $\hat{\mathbf{Q}}_n$ contains the resulting dispersion-free wavelet $\hat{q}\left(t_{ni};\ \hat{t}\right)$, as illustrated in Fig. 9(a).

A limitation for application of the dispersion removal procedure developed in this subsection is that the source-receiver distance r_{ni} must be known. In the next subsection, a solution for this drawback will be given.

4.2. Time-variant convolution

In practice, we always deal with bounded plates where reflections generate a complex bending wave field $q(x_n,\ t)$ with overlapping dispersive wavelets according to Eq. (5b). As an example, Fig. 10(a) shows one trace of a simulated bending wave field in a steel plate (dispersion constant $\text{A} = 6.76\,\text{ms}^{-0.5}$) consisting of a direct wavelet and two reflections, together with the amplitude spectrum of the direct wavelet (central frequency 2.5 kHz). The wavelets cannot be recognized individually. If, besides the model of Eq. (2d), the geometry of the plate and the positions of source and receivers are exactly known, the positions of the mirror image sources could be determined and for each relevant r_{ni} and t_{ni} an operator $f(t_{ni};\ t)$ could be calculated. As shown in Fig. 10(b), convolution of dataset $q(x_n,\ t)$ with such a filter yields dispersion removal for the wavelet with corresponding t_{ni}, in this case the direct wavelet, the amplitude spectrum of which remains unaffected. The other wavelets still appear in dispersive form, until the moment that the dataset is processed with the wavelet

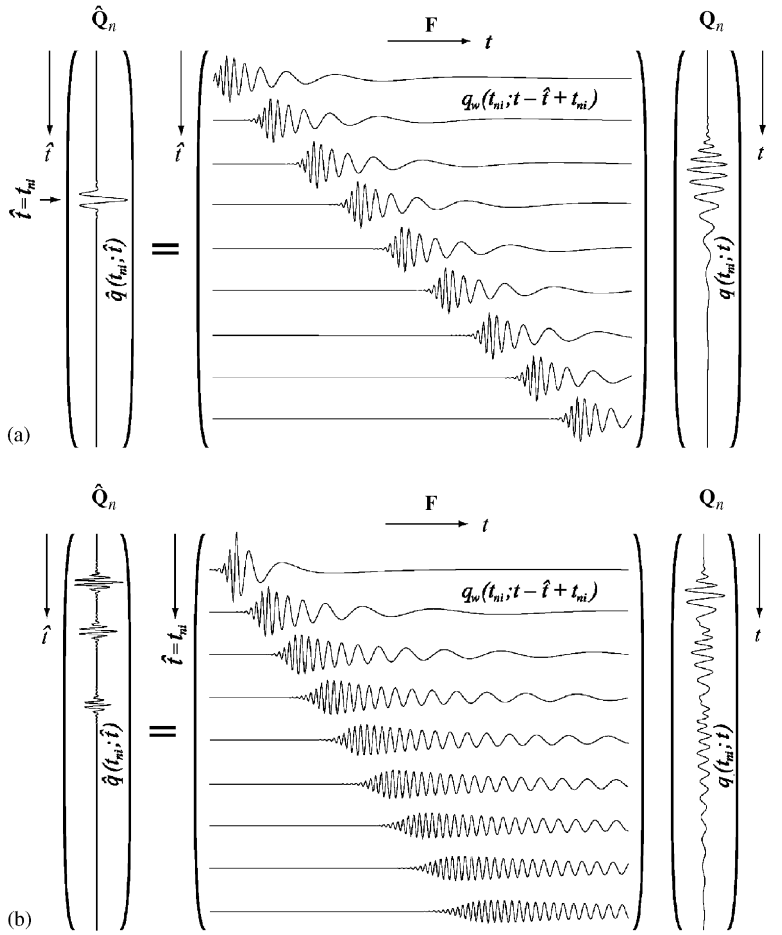

Fig. 9. Matrix representation of the time-invariant (a) and the time-variant (b) dispersion removal convolution process.

corresponding with their t_{ni} values. If after dispersion removal a wavelet is resolved from the other events in the dataset as in Fig. 10(b), it could be isolated, removed from the dataset and stored at the proper position in the substitute traveltime domain. This way, a dispersion-free dataset $\hat{q}(x_n, \hat{t})$ could be built up. However, reflection density increases with traveltime such that wavelet isolation and removal is not possible for higher order reflections and dispersion removal by time-invariant convolution will not work.

A better alternative here is dispersion removal by *time-variant* convolution. Then, beside the velocity model only the global geometry of the plate has to be known such that, for the substitute velocity to be chosen, the relevant region of t_{ni}-values can be determined. For a quasi-continuous distribution of t_{ni}-values in this region an operator $f(t_{ni}; t)$ is modeled and the convolution of each operator with the *complete* dataset $q(x_n; t)$ is calculated according to Eqs. (7f, 7g). But now, instead of for all values of $\hat{t}$, only the resulting value for $\hat{t} = t_{ni}$ is stored for each operator $f(t_{ni}; t)$. Hence, convolution of the dataset $q(x_n, t)$ with the operator modeled for a certain value of t_{ni} contributes one data point of a dispersion-free dataset in the substitute traveltime domain according to

$$\begin{aligned}\hat{q}(x_n, \hat{t} = t_{ni}) &= \int_{-\infty}^{+\infty} f(t_{ni}; t_{ni} - t) q(x_n, t)\,\mathrm{d}t \\ &= \int_{-\infty}^{+\infty} g(t_{ni}; -t) q(x_n, t)\,\mathrm{d}t \\ &= \int_{-\infty}^{+\infty} q_w(t_{ni}; t) q(x_n, t)\,\mathrm{d}t. \end{aligned} \tag{8a}$$

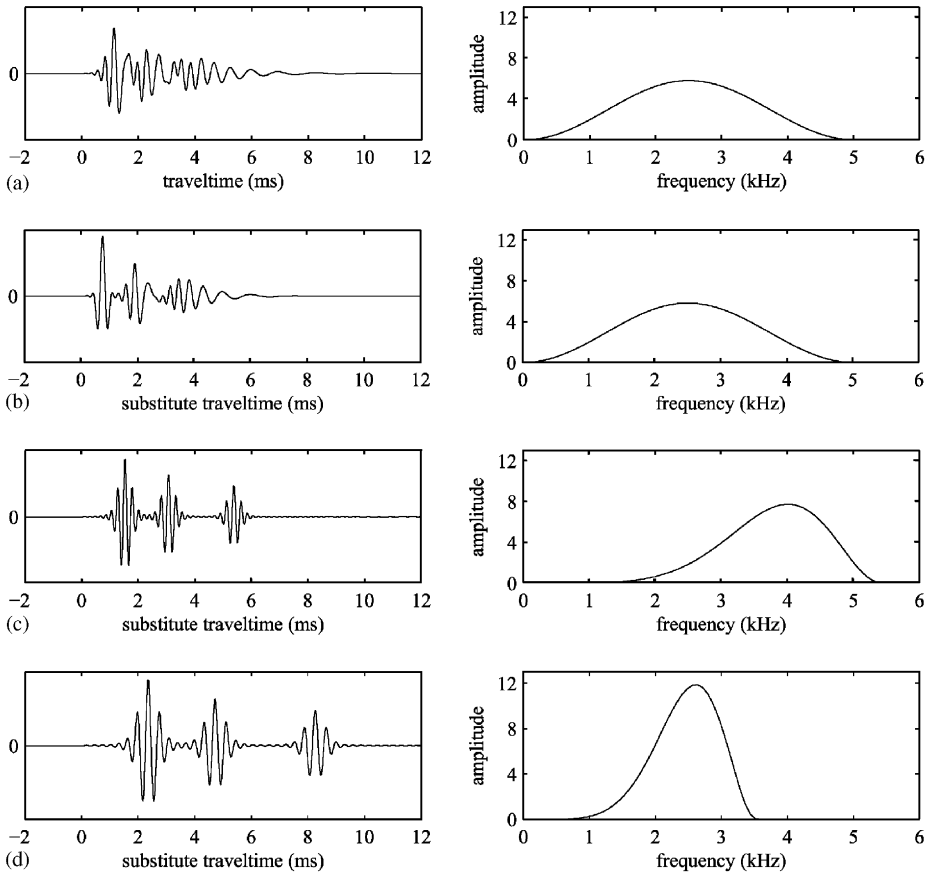

Fig. 10. (a) Direct bending wavelet and two reflections in steel ($r = [2,4,7]$ m, $A = 6{,}76\,\mathrm{m\,s^{-0.5}}$) with the amplitude spectrum of the direct wavelet only, (b) time-invariant convolution of the data set in (a) only one wavelet is dispersion-free; its amplitude spectrum is unaffected, (c) time-variant convolution of the data set in (a) with arbitrarily chosen substitute velocity $\hat{c} = 1300\,\mathrm{m\,s^{-1}}$: all wavelets are dispersion-free; the amplitude spectrum (again shown for the direct wave only) has been changed and (d) as (c), only now the substitute velocity $\hat{c}$ is chosen such that the peak of the amplitude spectrum (right) is located at the same frequency as for the original data, here at $f_c = 2.5\,\mathrm{kHz}$.

It is seen that this time-variant convolution can also be interpreted as taking the inner product of the complete dataset with a whitened version of the bending wavelet generated by a possible image source i. Only if this image source is really present, providing a contribution to the dataset $q(x_n, t)$, the inner product will have a significant value. The full dispersion-free dataset is obtained by summing these data points for all i:

$$\hat{q}(x_n, \hat{t}) = \sum_i \hat{q}(x_n, \hat{t} = t_{ni}). \tag{8b}$$

Fig. 10(c) shows the result of this time-variant convolution procedure for the dataset of Fig. 10(a), where, as before, substitute velocity $\hat{c}$ has been chosen 1300 m/s. The direct wavelet and the two reflections are now represented by dispersion-free versions, positioned at substitute traveltimes corresponding with the positions of their sources and the value of $\hat{c}$. However, the amplitude spectrum of the direct wavelet—and the reflections as well—has now been strongly changed. In the appendix it will be explained that the time-variant convolution described above introduces an asymmetric scaling in amplitude and frequency. Exact preservation of the original signal spectrum is not possible. However, it is possible to let the convolved wavelet have the same central frequency as the input data, and thus preserving the original spectrum by good approximation, if $\hat{c}$ is chosen equal to the propagation velocity of the central frequency component: $\hat{c} = A\sqrt{\omega_c}$. The convolved data with this choice of $\hat{c}$ is shown in Fig. 10(d). In the following, this choice of $\hat{c}$ will be made for all dispersion removal operations.

Also the time-variant dispersion removal operation can be elegantly represented in the vector–matrix notation of Eq. (7i) for each detector array element n. Now, column vector $\mathbf{Q}_n$ contains the complete input dataset $q(x_n, t)$, the rows of matrix $\mathbf{F}$ contain, for subsequent values of , $\hat{t} = t_{ni}$ the wavelets $q_w(t_{ni} = \hat{t}; t)$ and column vector $\hat{Q}_n$ contains the resulting dispersion-free dataset $\hat{q}(x_n, \hat{t})$, as illustrated in Fig. 9(b).

5. Dispersion removal results

5.1. Simulated array responses

In Section 3 (Fig. 6) the bending wave response in a rectangular steel plate was numerically simulated; the result is displayed again in Fig. 11(a). Fig. 11(b) shows the same dataset after application of the time-variant dispersion removal convolution procedure described in Section 4. The substitute propagation velocity has been chosen according to $\hat{c} = A\sqrt{\omega_c}$ so that the central frequency of the dispersion-free wavelet spectrum is the same as that of the original spectrum; cf. Fig. 10(d). Now, an increased temporal resolution is obtained, such that the direct and reflected wave fronts can be individually distinguished.

5.2. Measured array responses

Measurements have been performed on a free-hanging steel plate with the same thickness and dimensions as used in the simulations. Six source positions have been chosen as indicated in Fig. 12 which also specifies the

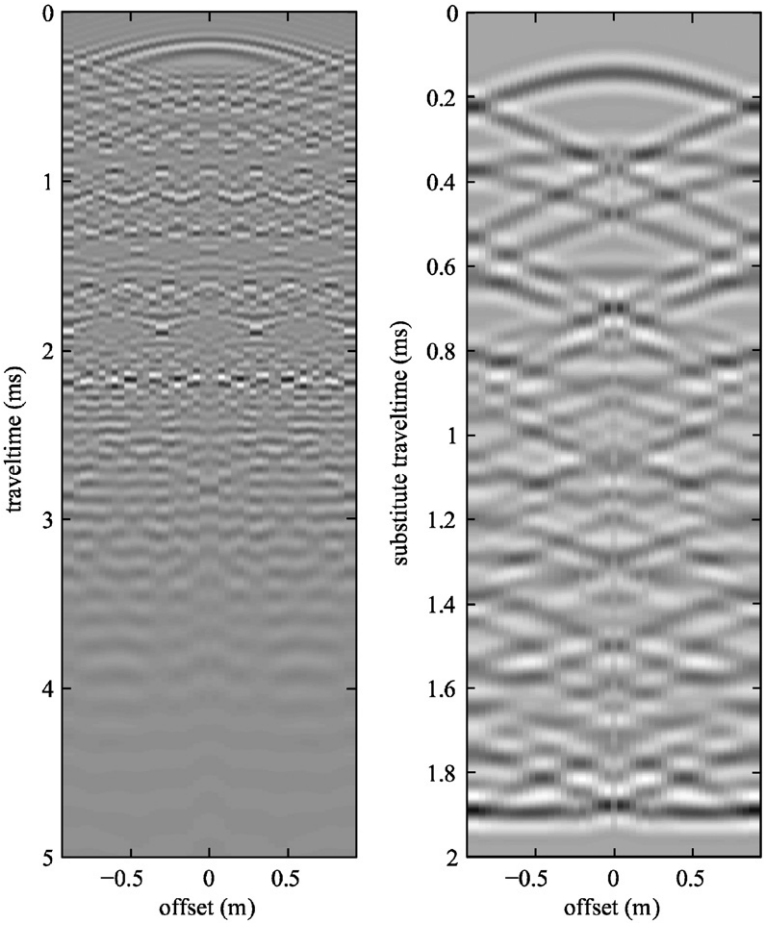

Fig. 11. Simulated bending wave field in a steel plate before (left) and after (right) dispersion removal.

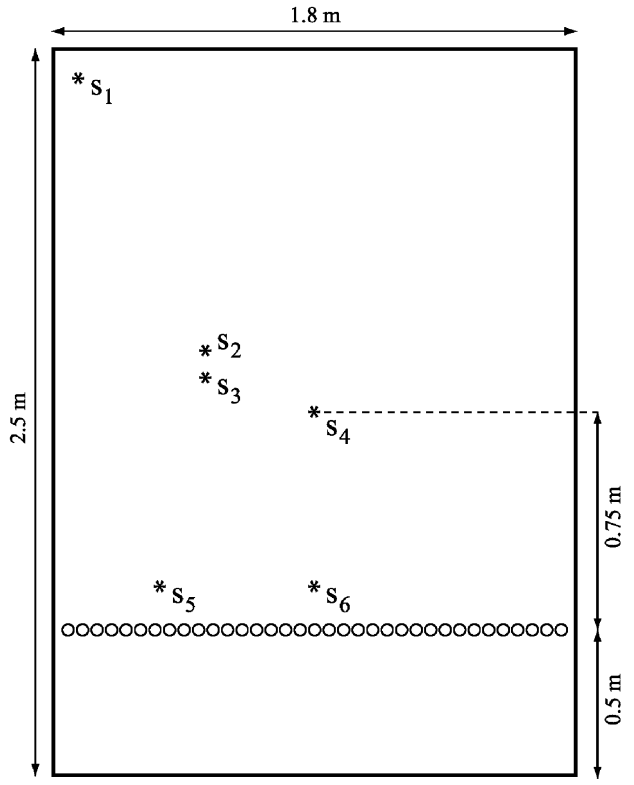

Fig. 12. Measurement configuration of the steel plate with the detector array and the six source positions s_1–s_6.

detector array position; the distance between the array elements was chosen 5 cm. The exciter was an impact hammer (Brüel & Kjaer type 8202), generating a pulse signal with a bandwidth roughly similar to the one used in the simulations. Since a hand-generated pulse is not repeatable, the source function was normalized by deconvolving the measured data with the actual source signal measured with the hammer device. (The measurements have been done in a reciprocal way: the plate was excited with the impact hammer at the 'detector' positions, whereas accelerometers were fixed at the 'source' positions. In the text, however, source and detector positions are denoted as in Fig. 12 for compatibility with the other configurations discussed in this paper.)

Fig. 13(a) shows an offset-traveltime representation for each source position separately. Even more than in the simulations, the wave fronts interfere such strongly that they cannot be distinguished separately. Fig. 13(b) shows the datasets after dispersion removal, displayed in the offset-(substitute) traveltime domain. Now, several wave fronts can be identified. In Fig. 14(a) the *simulated* quasi-longitudinal response of source #1 is shown, to be compared with the *measured* response after dispersion removal in Fig. 14(b). The similarity is satisfactory.

6. Conclusions and future research

6.1. Conclusions

By applying a convolution algorithm, dispersion can be removed from bending wave datasets, such that a dispersion-free version results, to which processing operations can be applied as developed for acoustic wave field analysis. For the hypothetical situation that all image source positions are known in advance and well-resolved, a time-invariant convolution operator can be used which leaves the amplitude spectra of the source

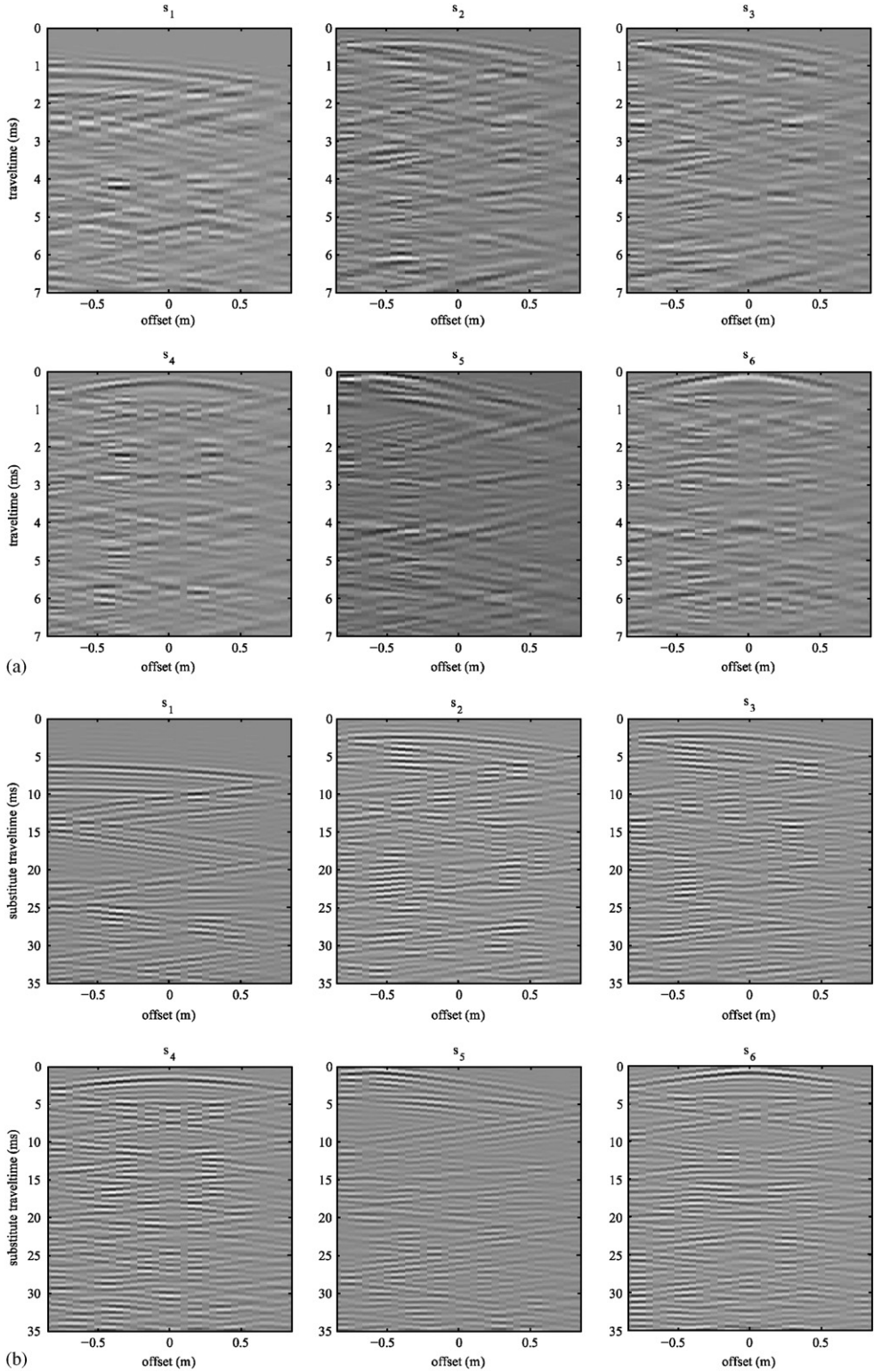

Fig. 13. Unprocessed (a) and processed (b) measurements on a steel plate (configuration Fig. 12). Note the significant improvement in resolution.

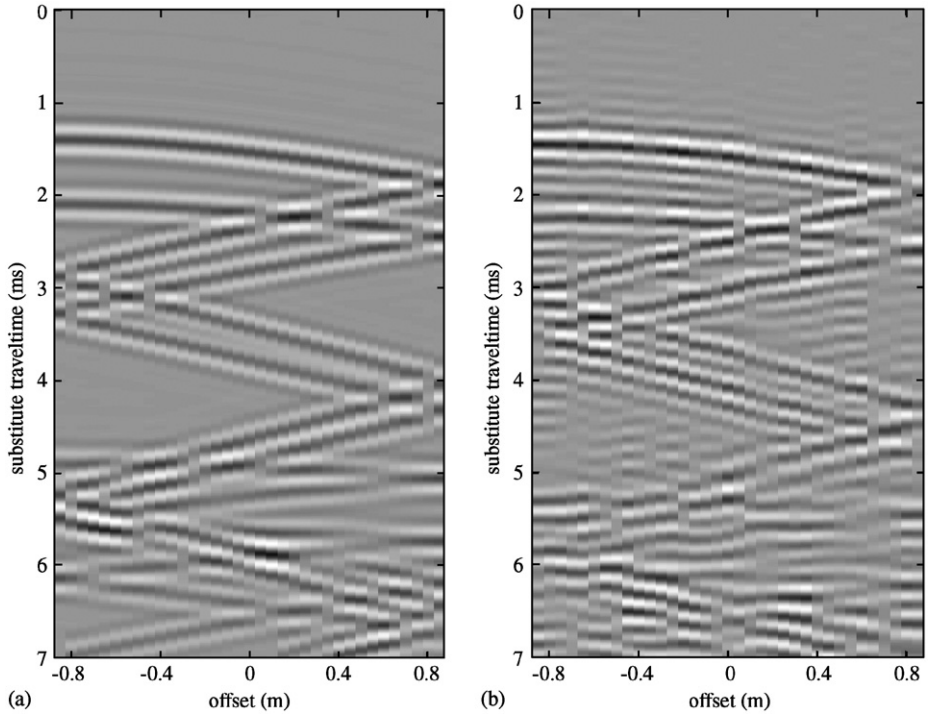

Fig. 14. Comparison between numerical simulation (a) and processed measurement (b) for source position s_1.

signals unaffected. For the practical situation that the image source positions are not known and the image source configuration has a high spatial density, a time-variant convolution operator has to be used which affects the amplitude spectra of the source signals, since dispersion removal is now implicitly coupled with frequency scaling.

The spectrum of the resulting dispersion-free waves can be optimized by choosing the substitute propagation velocity value in the time-variant convolution operator equal to the bending wave velocity at the central frequency of the original source spectrum. The proposed dispersion removal method has been validated with simulated and measured datasets; the performance is satisfactory.

6.2. Future research

The dispersion removal method has to be further tested and optimized for application in practical situations. The developed procedure can not only be applied to bending waves of which the propagation velocity is proportional to the square root of frequency, but to all dispersive wave types of which the velocity model is known. This has to be further evaluated.

Research has to be done to make the dispersion removal method adaptive, for application in situations where the velocity model is not known.

Acknowledgments

The authors want to express their thanks to Jan Martens for the preparing work that he did for this study, Jan Baan for his helpful comments and Lars Hörchens for his valuable support in the revision of the paper.

Appendix

In Fig. 10 it was seen that dispersion removal by time-variant convolution modifies the amplitude spectrum of the dataset. The spectral changes—which were not intended when developing the dispersion removal method—can be explained as follows.

From Eq. (8a) it follows that $\hat{q}(x_n, \hat{t})$ is the inverse Fourier transform of the product of $Q(x_n, \omega)$ and $F(t_{ni} = \hat{t}; \omega)$, such that using Eq. (7e) we write

$$\begin{aligned}\hat{q}(x_n, \hat{t}) &= \frac{1}{2\pi}\int_{-\infty}^{+\infty} Q(x_n, \omega) F(\hat{t}; \omega) \mathrm{e}^{\mathrm{j}\omega\hat{t}}\, \mathrm{d}\omega \\ &= \frac{1}{2\pi}\int_{-\infty}^{+\infty} Q(x_n, \omega) \mathrm{e}^{\mathrm{j}\omega(\hat{c}/c_b)\hat{t}}\, \mathrm{d}\omega. \end{aligned} \tag{A.1a}$$

To have the same amplitude spectrum as the original bending wave, the dispersion-free wave should just be the inverse Fourier transform of $Q(x_n, \omega)$, which it apparently is not. Instead, it is the inverse Fourier transform of a function $Q'(x_n, \omega')$ such that

$$\hat{q}(x_n, \hat{t}) = \frac{1}{2\pi}\int_{-\infty}^{+\infty} Q'(x_n, \omega') \mathrm{e}^{\mathrm{j}\omega'\hat{t}}\, \mathrm{d}\omega'. \tag{A.1b}$$

Comparison of Eqs. (A.1a) and (A.1b), and substitution of Eq. (2d) yields

$$\omega' = \frac{\hat{c}}{c_b}\omega = \frac{\hat{c}}{A}\sqrt{\omega} \tag{A.2a}$$

and hence

$$\mathrm{d}\omega' = \frac{\hat{c}}{2A\sqrt{\omega}}\mathrm{d}\omega. \tag{A.2b}$$

This means that $\hat{q}(x_n, \hat{t})$ is the inverse Fourier transform of a version of $Q(x_n, \omega)$ that is asymmetrically scaled in amplitude and frequency:

$$\begin{aligned} Q'(x_n, \omega') &= \frac{2A}{\hat{c}}\sqrt{\omega}\, Q(x_n, \omega) \\ &= 2\left(\frac{A}{\hat{c}}\right)^2 \omega'\, Q\left(x_n, \left(\frac{A}{\hat{c}}\omega'\right)^2\right) = \hat{Q}(x_n, \omega). \end{aligned} \tag{A.2c}$$

The amplitude scaling can be compensated by appropriate filtering if required. The frequency scaling, however, cannot fully be corrected in a simple way. A way to approximately preserve the original source spectrum is to choose the substitute velocity $\hat{c}$ such that the central frequency is kept in place after dispersion removal:

$$\hat{c} = A\sqrt{\omega_c} = c_B(\omega_c). \tag{A-3}$$

References

[1] R.H. Lyon, G. Maidanik, Power flow between linearly coupled oscillators, *Journal of the Acoustical Society of America* 34 (1962) 623–629.

[2] P.J. Holmes, The experimental characterization of wave propagation systems: II—continuous systems and the effects of dispersion, *Journal of Sound and Vibration* 35 (1974) 277–297.

[3] A. Chaigne, C. Lambourg, Time-domain simulation of damped impacted plates. I. Theory and experiments, *Journal of the Acoustical Society of America* 109 (2001) 1422–1432.

[4] S. Schedin, C. Lambourg, A. Chaigne, Transient sound fields from impacted plates: comparison between numerical simulations and experiments, *Journal of Sound and Vibration* 221 (1999) 471–490.

[5] A.J. Berkhout, D. de Vries, J.J. Sonke, Array technology for acoustic wavefield analysis in enclosures, *Journal of the Acoustical Society of America* 102 (1997) 2757–2770.

[6] A.J. Berkhout, M.M. Boone, P.J.M. Valks, Multichannel impulse responses for outdoor sound propagation, *Journal of the Acoustical Society of America* 98 (1995) 1169–1177.
[7] A.J. Berkhout, Related properties of minimum-phase and zero-phase time functions, *Geophysical Prospecting* 22 (1974) 683–709.
[8] L. Cremer, M. Heckl, E.E. Ungar, *Structure-Borne Sound*, Springer, Berlin/Heidelberg/New York, 1973.